THIRD EDITION

Radiogenic Isotope Geology

ALAN P. DICKIN

Radiogenic Isotope Geology

Third Edition

The third edition of *Radiogenic Isotope Geology* examines revolutionary changes in geochemical thinking that have occurred over the past 15 years. Extinct nuclide studies on meteorites have called into question fundamental geochemical models of the Earth, while new dating methods have challenged conventional views of Earth history. At the same time, the problem of global warming has raised new questions about the causes of past and present climate change. In the new edition, these and other recent issues are evaluated in their scholarly and historical context, so readers can understand the development of current ideas. Controversial theories, new analytical techniques, classic papers, and illustrative case studies all come under scrutiny in this book, providing an accessible introduction for students and critical commentary for researchers.

Alan P. Dickin is Professor of Geology at McMaster University.

"The Dickin text provides an excellent introduction to radiogenic isotope geochemistry. I read a previous edition cover-to-cover during preparation for the general knowledge exams in graduate school, and I still suggest that graduate students do the same in preparation for their exams. It continues to be a key reference for teaching and in the classroom and in the laboratory."

– *Matthew Jackson, University of California, Santa Barbara*

"Isotope geochemistry is hugely influential in the development of new approaches and ideas in the Earth sciences. New data challenge models for the formation of the Earth, the evolution of the continental crust, and climate change. An understanding of the basic principles of isotope geology is important in a wide range of the sciences, and this welcome third edition of *Radiogenic Isotope Geology* builds on the success of the previous editions. It is scholarly and accessible, and it combines an all too rare historical context with a comprehensive introduction to a wide range of radiogenic isotope techniques. Written by one of the world's most respected authors in this field, this textbook will be invaluable for undergraduate and graduate courses, and it is an excellent reference text for scientists in other fields."

– *Chris Hawkesworth, University of Bristol*

"For teachers and students in both low- and high-temperature geochemistry who need ready access to geochemical concepts and techniques, Alan Dickin offers an up-to-date, well-written medium-level textbook on isotope geochemistry. A pleasant, handy, and useful book for your shelf."

– *Francis Albarède, Ecole Normale Supérieure de Lyon*

Radiogenic Isotope Geology

Third Edition

Alan P. Dickin
McMaster University

CAMBRIDGE
UNIVERSITY PRESS

CAMBRIDGE
UNIVERSITY PRESS

University Printing House, Cambridge CB2 8BS, United Kingdom

One Liberty Plaza, 20th Floor, New York, NY 10006, USA

477 Williamstown Road, Port Melbourne, VIC 3207, Australia

314-321, 3rd Floor, Plot 3, Splendor Forum, Jasola District Centre, New Delhi - 110025, India

79 Anson Road, #06-04/06, Singapore 079906

Cambridge University Press is part of the University of Cambridge.

It furthers the University's mission by disseminating knowledge in the pursuit of education, learning and research at the highest international levels of excellence.

www.cambridge.org
Information on this title: www.cambridge.org/9781107099449
DOI: 10.1017/9781316163009

First published 1995
Second edition published 2005
Third edition published 2018

Printed in the United States of America by Sheridan Books, Inc. 2018

A catalogue record for this publication is available from the British Library

Library of Congress Cataloging-in-Publication data
Names: Dickin, Alan P., author.
Title: Radiogenic isotope geology / Alan P. Dickin, McMaster University.
Description: [2018 edition]. | Cambridge : Cambridge University Press, 2018. | Includes bibliographical references and index.
Identifiers: LCCN 2017023083 | ISBN 9781107099449 (alk. paper)
Subjects: LCSH: Isotope geology. | Radioactive dating. | Geochemistry. | Paleoclimatology. | Environmental archaeology.
Classification: LCC QE501.4.N9 D53 2017 | DDC 551.9–dc23
LC record available at https://lccn.loc.gov/2017023083

ISBN 978-1-107-09944-9 Hardback
ISBN 978-1-107-49212-7 Paperback

Additional resources for this publication at www.cambridge.org/dickin3

To Margaret
and to the memory of Stephen Moorbath,
isotope pioneer

Contents in Brief

Contents

Preface and Acknowledgements

The past fifteen years have seen a quiet revolution in isotope geochemistry, as a once-arcane field involving 'extinct' radionuclides in meteorites has called into question fundamental geochemical models of the Earth itself. At the same time, increasing public awareness of the problem of anthropogenic global warming has focused attention on the role of isotope geochemistry in monitoring past and present influences on climate change.

The third edition of *Radiogenic Isotope Geology* attempts to place these and other recent developments in scientific thinking in their overall scholarly context.

The approach to the subject matter is historical, for three main reasons. Firstly, to give an impression of the development of thought in the field so that the reader can understand the origin of present ideas; secondly, to explain why past theories have had to be modified; and thirdly, to present 'fall back' positions lest current models be refuted at some future date. This approach embodies the scholarly principle that knowledge of the classic work in the field is the starting point for current research.

The text is also particularly focussed on three types of literature. Firstly, it attempts to give accurate attribution of new ideas or methods; secondly, it reviews classic papers which have become standards in their field; and thirdly, it presents case studies that have evoked controversy in the literature, as examples of alternative data interpretations.

The organization of the book allows each chapter to be a relatively free-standing entity covering one segment of the field of radiogenic isotope geology. However, the reader may benefit from an understanding of the thread, which, in the author's mind, links these chapters together.

Chapter 1 introduces radiogenic isotopes by discussing the synthesis and decay of nuclides within the context of nuclear stability. Decay constants and the radioactive decay law are introduced.

Chapter 2 provides an experimental background to many of the chapters that follow by discussing the details of mass spectrometric analysis (TIMS and ICP–MS), along with a discussion of isochron regression fitting.

The next three chapters introduce the three pillars of lithophile isotope geology, comprising the Sr, Nd and Pb isotope methods. Emphasis is placed on their applications to geochronology and their evolution in terrestrial systems. Chapter 3 covers the Rb–Sr system, since this is one of the simplest and most basic dating methods. Chapter 4 covers the Sm–Nd system, including the use of Nd model ages to date crustal formation. Chapter 5 examines U–Pb geochronology and introduces the complexities of terrestrial Pb isotope evolution in a straightforward fashion. Each chapter ends with an examination of these isotopes as environmental tracers, focussing particularly on the oceans.

Chapters 6 and 7 apply Sr, Nd and Pb, as geochemical tracers, to the study of oceanic and continental igneous rocks. This is appropriate, because these isotopes are some of the basic tools of the isotope geochemist, which together may allow understanding of the complexities of mantle processes and magmatic evolution. These methods are supplemented in Chapters 8 and 9 by insights from the Re–Os, Lu–Hf and other lithophile isotope systems, which arise from their distinct chemistry.

Chapter 10 completes the panoply of long-lived isotopic dating systems by introducing the K–Ar, Ar–Ar and U–He methods, including their applications to magnetic and thermal histories. This leads us naturally in Chapter 11 to the consideration of rare gases as isotopic tracers, which give unique insights into the de-gassing history of the Earth.

Chapter 12 introduces the short-lived isotopes of the uranium decay series, covering classical and recent developments in the dating of Quaternary-age sedimentary rocks. This prepares us for the complexities of Chapter 13, which examines U-series isotopes as tracers in igneous systems. Short-lived processes in mantle melting and magma evolution are the focus of attention here.

Chapter 14 examines the most important of the cosmogenic isotopes. These represent a vast and growing field of chronology and isotope chemistry, which is especially pertinent to environmental geoscience. In particular, the radiocarbon method is a vital dating tool in archaeology and a tracer of the ocean–atmosphere system involved in climate change.

Chapter 15 represents a comprehensive review of the 'extinct nuclide' systems in meteorites that have recently raised questions about the cosmic context of terrestrial geochemistry. This overview deals with all of the major extinct nuclide pairs, and discusses their significance for the origins of the solar system and the Earth.

Lastly, Chapter 16 examines the specialized field of (radiogenic) fission track analysis, originally developed as a regular dating method, but increasingly applied to thermal history analysis.

The text is gathered around a large number of diagrams, many of which are classic figures from the literature. I gratefully acknowledge the many authors whose original data and diagrams form the basis for these figures. Author acknowledgement for all figure sources is given within individual figure captions, and corresponding titles, journal names, volumes and pages are contained in the list of cited references at the end of each chapter.

Alan P. Dickin
McMaster University

Chapter 1

Nucleosynthesis and Nuclear Decay

1.1 The Chart of the Nuclides

In the field of isotope geology, neutrons, protons and electrons can be regarded as the fundamental building blocks of the atom. The composition of a given type of atom, called a nuclide, is described by specifying the number of protons (atomic number, *Z*) and the number of neutrons (*N*) in the nucleus. The sum of these is the mass number (*A*). By plotting *Z* against *N* for all of the nuclides that have been known to exist (at least momentarily), the chart of the nuclides is obtained (Fig. 1.1). In this chart, horizontal rows of nuclides represent the same element (constant *Z*) with a variable number of neutrons (*N*). These are isotopes.

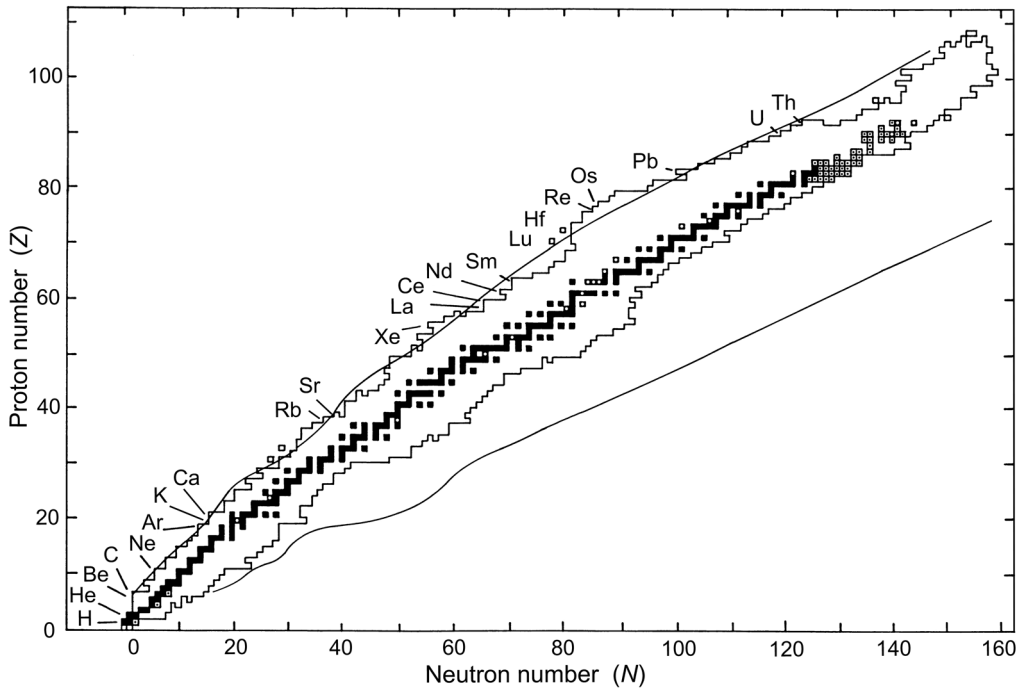

Fig. 1.1 Chart of the nuclides in coordinates of proton number *Z*, against neutron number *N*. (■) = stable nuclides; (□) = unstable nuclides; (◘) = naturally occurring long-lived unstable nuclides; (⊡) = naturally occurring short-lived unstable nuclides. Some geologically useful radionuclides are marked. Smooth envelope = theoretical nuclide stability limits. For a more detailed nuclide chart, see Appendix 1.

A botal of 264 stable nuclides are known, which have not been observed to decay with available detection equipment. These define a central 'path of stability', coloured black in Fig. 1.1. On either side of this path, the zig-zag outline defines the limits of experimentally known unstable nuclides compiled by Hansen (1987). These species tend to undergo increasingly rapid decay as one moves out on either side of the path of stability. The smooth outer envelopes are the theoretical limits of nuclide stability ('drip lines') beyond which prompt decay occurs. This means that the synthesis and decay of an unstable nuclide occurs in a single particle interaction, giving it a zero effective lifetime.

As work progresses, the domain of experimentally known nuclides should approach the theoretical envelope, as has already occurred for nuclides with $Z < 20$ (Thoennessen, 2013). This has been achieved over the past 60 years using heavy ion accelerators (e.g. Darmstadt) to make exotic species by collision. Because of the curvature of the path of stability (Fig. 1.1), it was relatively easy to populate the proton-rich side of the path of stability, since these species can be made by fusion of lighter elements. Species on the neutron-rich side are made by bombarding target material with ^{238}U, creating unstable heavy atoms which immediately undergo fission to produce very neutron-rich products (e.g. Geissel *et al*., 2003). Knowledge about these unstable nuclei will improve our understanding of the nucleosynthetic r-process which occurs in supernovae (Thoennessen and Sherrill, 2011).

A small number of unstable nuclides have sufficiently long half-lives that they have not entirely decayed to extinction since the formation of the solar system. A few other short-lived nuclides are either continuously generated in the decay series of uranium and thorium, or produced by cosmic ray bombardment of stable nuclides. These nuclides, and one or two extinct short-lived isotopes, plus their daughter products, are the realm of radiogenic isotope geology. Those with half-lives over 0.5 Ma are marked in Fig. 1.2. Nuclides with half-lives over 1000 Ga decay too slowly to be geologically useful. Observation shows that all of the other long-lived isotopes either have been or are being applied in geology.

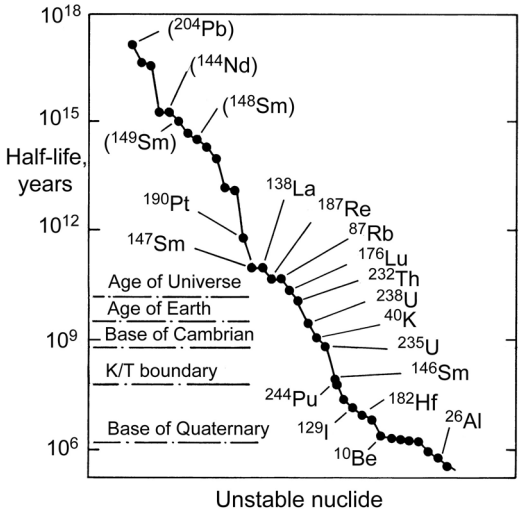

Fig. 1.2 Unstable nuclides with half-lives ($t_{1/2}$) over 0.5 Ma, in order of decreasing stability. Geologically useful parent nuclides are marked. Some very long-lived radionuclides with no geological application are also marked in brackets.

1.2 Nucleosynthesis

A realistic model for the nucleosynthesis of the elements must be based on empirical data for their 'cosmic abundance'. True cosmic abundances can be derived from stellar spectroscopy or by chemical analysis of galactic cosmic rays. However, such data are difficult to measure at high precision, so cosmic abundances are normally approximated by solar-system abundances. These can be determined by solar spectroscopy or by direct analysis of the most 'primitive' meteorites, carbonaceous chondrites. A comparison of the latter two sources of data (Ross and Aller, 1976) demonstrates good agreement for most elements (Fig. 1.3). Exceptions are the volatile elements, which have been lost from meteorites, and the Li–Be–B group, which are unstable in stars.

It is widely believed (e.g. Weinberg, 1977) that about 30 minutes after the 'big bang', the matter of the universe (in the form of protons and neutrons) consisted mostly of ^{1}H and 22–28% by mass of ^{4}He, along with traces of ^{2}H (deuterium) and ^{3}He. Hydrogen is still by far the most abundant element in the universe (88.6% of all nuclei) and with helium, makes up 99% of its mass, but naturally occurring heavy nuclides now exist up to atomic weight 254 or beyond

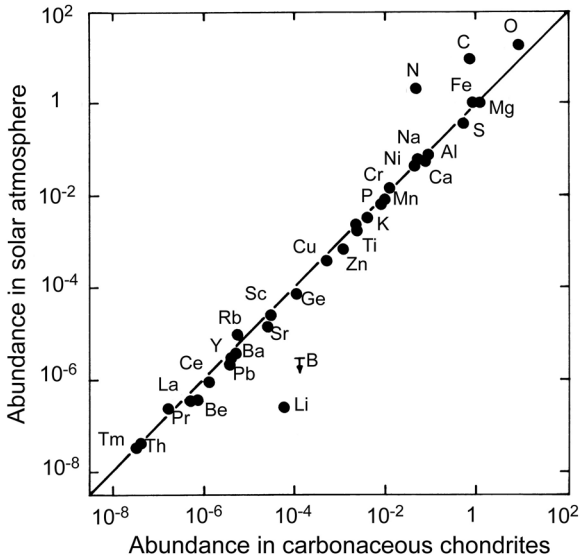

Fig. 1.3 Comparison of solar system abundances (relative to silicon) determined by solar spectroscopy and by analysis of carbonaceous chondrites. After Ringwood (1979).

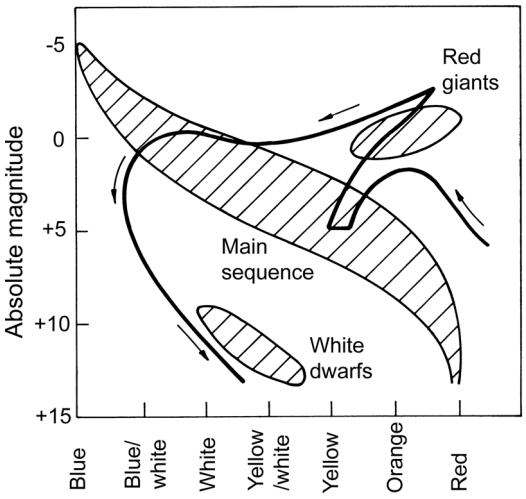

Fig. 1.4 Plot of absolute magnitude against spectral class of stars. Hatched areas show distributions of the three main star groups. The postulated evolutionary path of a star of solar mass is shown.

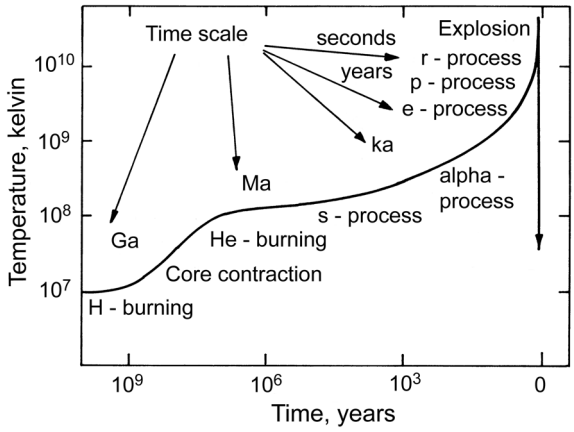

Fig. 1.5 Schematic evolution of a large star showing nucleosynthetic processes along its accelerating life-history in response to increasing temperature. Time is measured backwards from the end of the star's life on the right. After Burbidge *et al.* (1957).

(Fig. 1.1). These heavier nuclei must have been produced by nucleosynthetic processes in stars, and not in the big bang, because stars of different ages have different compositions which can be detected spectroscopically. Furthermore, stars at particular evolutionary stages may have compositional abnormalities, such as the presence of ^{254}Cf in supernovae. If nucleosynthesis of the heavy elements had occurred in the big bang then their distribution would be uniform about the universe.

1.2.1 Stellar Evolution

Present day models of stellar nucleosynthesis are based heavily on a classic review paper by Burbidge *et al.* (1957), in which eight element-building processes were identified (hydrogen burning, helium burning, α, e, x, r, s and p). Different processes were invoked to explain the abundance patterns of different groups of elements. These processes are, in turn, linked to different stages of stellar evolution. It is therefore appropriate at this point to summarize the life-history of some typical stars (e.g. Iben, 1967). The length of this life-history depends directly on the stellar mass, and can be traced on a plot of absolute magnitude (brightness) against spectral class (colour), referred to as the Hertzsprung–Russell or H–R diagram (Fig. 1.4).

Gravitational accretion of a star of solar mass from cold primordial hydrogen and helium would probably take about 1 Ma to raise the core temperature to ca. 10^7 K, when nuclear fusion of hydrogen to helium can begin (Atkinson and Houtermans, 1929). This process is also called 'hydrogen burning'. The star spends most of its life at this stage, as a 'main sequence' star, where an equilibrium is set up between energy supply by fusion and energy loss in the form of radiation. For the Sun, this stage will probably last ca. 10 Ga, but a very large star with 15 times the Sun's mass may remain in the main sequence for only 10 Ma.

When the bulk of hydrogen in a small star has been converted into ^{4}He, inward density-driven forces exceed outward radiation pressure, causing gravitational contraction. However, the resulting rise in core temperature causes expansion of the outer hydrogen-rich layer of the star. This forms a huge low-density envelope whose surface temperature may fall to ca. 4000 K, observed as a 'red giant'. This stage lasts only one tenth as long as the main sequence stage. When core temperatures reach 1.5×10^7 K, a more efficient hydrogen-burning reaction becomes possible if the star contains traces of carbon, nitrogen and oxygen inherited from older generations of stars. This form of hydrogen burning is called the C–N–O cycle (Bethe, 1939).

At some point during the red giant stage, core temperatures may reach 10^8 K, when helium fusion to carbon is ignited (the 'helium flash'). Further core contraction, yielding a temperature of ca. 10^9 K, follows as helium becomes exhausted. At these temperatures an endothermic process of α-particle emission can occur, allowing the building of heavier nuclides up to mass 40. However, this quickly expends the remaining burnable fuel of the star, which then cools to a white dwarf.

More massive stars (of several solar masses) have a different life-history. In these stars, greater gravitationally induced pressure–temperature conditions allow the fusion of helium to begin early in the red giant stage. This is followed by further contraction and heating, allowing the fusion of carbon and successively heavier elements. However, as lighter elements become exhausted, gravitationally induced contraction and heating occur at an ever increasing pace (Fig. 1.5), until the implosion is stopped by the attainment of neutron-star density. The resulting shock wave causes a

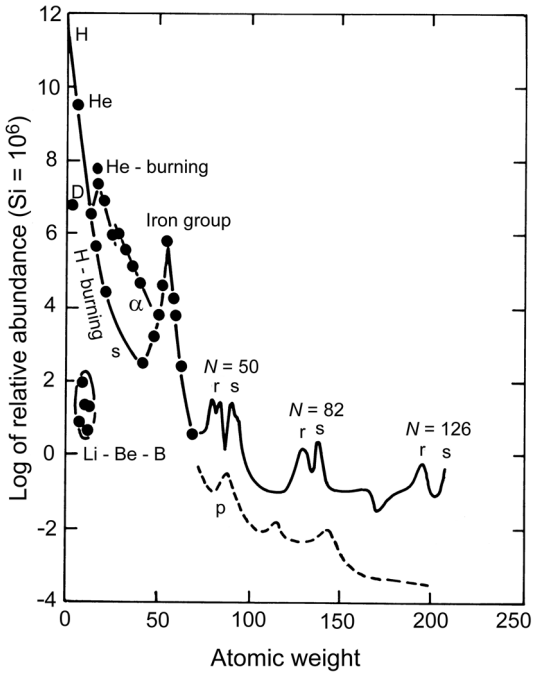

Fig. 1.6 Schematic diagram of the cosmic abundances of the elements, highlighting the nucleosynthetic processes responsible for forming different groups of nuclides. After Burbidge *et al.* (1957).

supernova explosion which ends the star's life (e.g. Burrows, 2000).

In the minutes before explosion, when temperatures exceed 3×10^9 K, very rapid nuclear interactions occur. Energetic equilibrium is established between nuclei and free protons and neutrons, synthesizing elements like Fe by the so-called e-process. The supernova explosion itself lasts only a few seconds, but is characterized by colossal neutron fluxes. These very rapidly synthesize heavier elements, terminating at ^{254}Cf, which undergoes spontaneous fission. Products of the supernova explosion are distributed through space and later incorporated in a new generation of stars.

1.2.2 Stages in the Nucleosynthesis of Heavy Elements

A schematic diagram of the cosmic abundance chart is given in Fig. 1.6. We will now see how different nucleosynthetic processes are invoked to account for its form.

The element-building process begins with the fusion of four protons to one ^{4}He nucleus, which occurs in three stages:

$$^1\mathrm{H} + {}^1\mathrm{H} \rightarrow {}^2\mathrm{D} + \mathrm{e}^+ + \nu \qquad (Q = +1.44\,\mathrm{MeV},\ t_{1/2} = 14\,\mathrm{Ga})$$

$$^2\mathrm{D} + {}^1\mathrm{H} \rightarrow {}^3\mathrm{He} + \gamma \qquad (Q = +5.49\,\mathrm{MeV},\ t_{1/2} = 0.6\,\mathrm{s})$$

$$^3\mathrm{He} + {}^3\mathrm{He} \rightarrow {}^4\mathrm{He} + 2\,{}^1\mathrm{H} + \gamma \qquad (Q = +12.86\,\mathrm{MeV},\ t_{1/2} = 1\,\mathrm{Ma}),$$

where Q is the energy output and $t_{1/2}$ is the reaction time of each stage (the time necessary to consume one half of the reactants) for the centre of the Sun. The long reaction time for the first step explains the long duration of the hydrogen-burning (main sequence) stage for small stars like the Sun. The overall reaction converts four protons into one helium nucleus, two positrons and two neutrinos, plus a large output of energy in the form of high-frequency photons. Hence the reaction is very strongly exothermic. Although deuterium and ^{3}He are generated in the first two reactions above, their consumption in the third accounts for their much lower cosmic abundance than ^{4}He.

If heavier elements such as carbon and nitrogen are present in a star, the catalytic C–N–O sequence of reactions can occur, which also combines four protons to make one helium nucleus:

$$^{12}\mathrm{C} + {}^1\mathrm{H} \rightarrow {}^{13}\mathrm{N} + \gamma \qquad (Q = +1.95\,\mathrm{MeV},\ t_{1/2} = 13\,\mathrm{Ma})$$

$$^{13}\mathrm{N} \rightarrow {}^{13}\mathrm{C} + \mathrm{e}^+ + \nu \qquad (Q = +2.22\,\mathrm{MeV},\ t_{1.2} = 7\ \mathrm{min})$$

$$^{13}\mathrm{C} + {}^1\mathrm{H} \rightarrow {}^{14}\mathrm{N} + \gamma \qquad (Q = +7.54\,\mathrm{MeV},\ t_{1/2} = 3\,\mathrm{Ma})$$

$$^{14}\mathrm{N} + {}^1\mathrm{H} \rightarrow {}^{15}\mathrm{O} + \gamma \qquad (Q = +7.35\,\mathrm{MeV},\ t_{1/2} = 0.3\,\mathrm{Ma})$$

$$^{15}\mathrm{O} \rightarrow {}^{15}\mathrm{N} + \mathrm{e}^+ + \nu \qquad (Q = +2.70\,\mathrm{MeV},\ t_{1/2} = 82\,\mathrm{s})$$

$$^{15}\mathrm{N} + {}^1\mathrm{H} \rightarrow {}^{12}\mathrm{C} + {}^4\mathrm{He} \qquad (Q = +4.96\,\mathrm{MeV},\ t_{1/2} = 100\,\mathrm{ka}).$$

The C–N–O elements have greater potential energy barriers to fusion than hydrogen, so these reactions require higher temperatures to operate than the simple proton–proton (p–p) reaction. However, the reaction times are much shorter than for the p–p reaction. Therefore the C–N–O reaction contributes less than 10% of hydrogen-burning reactions in a small star like the Sun, but is overwhelmingly dominant in large stars. This explains their much shorter lifespan in the main sequence.

Helium burning also occurs in stages:

$$^4\mathrm{He} + {}^4\mathrm{He} \leftrightarrow {}^8\mathrm{Be} \qquad (Q = +0.09\,\mathrm{MeV})$$

$$^8\mathrm{Be} + {}^4\mathrm{He} \leftrightarrow {}^{12}\mathrm{C}^* \qquad (Q = -0.37\,\mathrm{MeV})$$

$$^{12}\mathrm{C}^* \rightarrow {}^{12}\mathrm{C} + \gamma \qquad (Q = +7.65\,\mathrm{MeV})$$

The ^{8}Be nucleus is very unstable ($t_{1/2} < 10^{-15}$ s) and in the core of a red giant the Be/He equilibrium ratio is estimated at 10^{-9}. However its life is just long enough to allow the possibility of collision with another helium nucleus. (Instantaneous three-particle collisions are very rare.) The energy yield of the first stage is small, and the second is actually endothermic, but the decay of excited ^{12}C* to the ground state is strongly exothermic, driving the equilibrium to the right.

The elements Li, Be and B have low nuclear binding energies, so that they are unstable at the temperatures of 10^7 K and above found at the centre of stars. They are therefore bypassed by stellar nucleosynthetic reactions, leading to low

cosmic abundances (Fig. 1.6). The fact that the five stable isotopes ^{6}Li, ^{7}Li, ^{9}Be, ^{10}B and ^{11}B exist at all has been attributed to fragmentation effects (spallation) of heavy cosmic rays (atomic nuclei travelling through the galaxy at relativistic speeds) as they hit interstellar gas atoms (Reeves, 1974). This is termed the x-process.

Problems have been recognized in the x-process model for generating the light elements Li, Be and B, since cosmic ray spallation cannot explain the observed isotope ratios of these elements in solar system materials. However, Casse *et al*. (1995) proposed that carbon and oxygen nuclei ejected from supernovae can generate these nuclides by collision with hydrogen and helium in the surrounding gas cloud. This process is believed to occur in regions such as the Orion nebula. The combination of supernova production with spallation of galactic cosmic rays can explain observed solar system abundances of Li, Be and B.

Following the synthesis of carbon, further helium-burning reactions are possible, to produce heavier nuclei:

$$^{12}\mathrm{C} + {}^{4}\mathrm{He} \rightarrow {}^{16}\mathrm{O} + \gamma \quad (Q = +7.15\,\mathrm{MeV})$$

$$^{16}\mathrm{O} + {}^{4}\mathrm{He} \rightarrow {}^{20}\mathrm{Ne} + \gamma \quad (Q = +4.75\,\mathrm{MeV})$$

$$^{20}\mathrm{Ne} + {}^{4}\mathrm{He} \rightarrow {}^{24}\mathrm{Mg} + \gamma \quad (Q = +9.31\,\mathrm{MeV})\,.$$

Intervening nuclei such as ^{13}N can be produced by adding protons to these species, but are themselves consumed in the process of catalytic hydrogen burning mentioned above.

In old red giant stars, carbon-burning reactions can occur:

$$^{12}\mathrm{C} + {}^{12}\mathrm{C} \rightarrow {}^{24}\mathrm{Mg} + \gamma \quad (Q = +13.85\,\mathrm{MeV})$$

$$\rightarrow {}^{23}\mathrm{Na} + {}^{1}\mathrm{H} \quad (Q = +2.23\,\mathrm{MeV})$$

$$\rightarrow {}^{20}\mathrm{Ne} + {}^{4}\mathrm{He} \quad (Q = +4.62\,\mathrm{MeV})\,.$$

The hydrogen and helium nuclei regenerated in these processes allow further reactions which help to fill in gaps between masses 12 and 24.

When a small star reaches its maximum core temperature of 10^9 K the endothermic α-process can occur:

$$^{20}\mathrm{Ne} + \gamma \rightarrow {}^{16}\mathrm{O} + {}^{4}\mathrm{He}\,(Q = -4.75\,\mathrm{MeV})\,.$$

The energy consumption of this process is compensated by strongly exothermic reactions such as:

$$^{20}\mathrm{Ne} + {}^{4}\mathrm{He} \rightarrow {}^{24}\mathrm{Mg} + \gamma\ (Q = +9.31\,\mathrm{MeV})\,,$$

so that the overall reaction generates a positive energy budget. The process resembles helium burning, but is distinguished by the different source of ^{4}He. The α-process can build up from ^{24}Mg through the sequence ^{28}Si, ^{32}S, ^{36}Ar and ^{40}Ca, where it terminates, owing to the instability of ^{44}Ti.

The maximum temperatures reached in the core of a small star do not allow substantial heavy element production. However, in the final stages of the evolution of larger stars, before a supernova explosion, the core temperature exceeds 3×10^9 K. This allows energetic equilibrium to be established by very rapid nuclear reactions between the various nuclei and free protons and neutrons (the e-process). Because ^{56}Fe is at the peak of the nuclear binding energy curve, this element is most favoured by the e-process (Fig. 1.6). However, the other first-series transition elements V, Cr, Mn, Co and Ni in the mass range 50 to 62 are also attributed to this process.

During the last few million years of a red giant's life, a slow process of neutron addition with emission of gamma rays (the s-process) can synthesize many additional nuclides up to mass 209 (see Fig. 1.7). Two possible neutron sources are:

$$^{13}\mathrm{C} + {}^{4}\mathrm{He} \rightarrow {}^{16}\mathrm{O} + \mathrm{n} + \gamma$$

$$^{21}\mathrm{Ne} + {}^{4}\mathrm{He} \rightarrow {}^{24}\mathrm{Mg} + \mathrm{n} + \gamma.$$

The ^{13}C and ^{21}Ne parents can be produced by proton bombardment of the common ^{12}C and ^{20}Ne nuclides.

Because neutron capture in the s-process is relatively slow, unstable neutron-rich nuclides generated in this process have time to decay by β emission before further neutron addition. Hence the nucleosynthetic path of the s-process climbs in many small steps up the path of greatest stability of proton/neutron ratio (Fig. 1.7) and is finally terminated by the α decay of ^{210}Po back to ^{206}Pb and ^{209}Bi back to ^{205}Tl.

The 'neutron capture cross-section' of a nuclide expresses how readily it can absorb incoming thermal neutrons, and therefore determines how likely it is to be converted to a higher atomic mass species by neutron bombardment. Nuclides with certain neutron numbers (e.g. 50, 82 and 126) have unusually small neutron capture cross-sections, making them particularly resistant to further reaction and giving rise to local peaks in abundance at masses 90, 138 and 208. Hence, $N = 50$, 82 and 126 are empirically referred to as neutron 'magic numbers'.

In contrast to the s-process, which may occur over periods of millions of years in red giants, r-process neutrons are added in very rapid succession to a nucleus before β decay is possible. The nuclei are therefore rapidly driven to the neutron-rich side of the stability line, until they reach a new equilibrium between neutron addition and β decay, represented by the hatched zone in Fig. 1.7. Nuclides move along this r-process pathway until they reach a configuration with low neutron capture cross-section (a neutron magic number). At these points a 'cascade' of alternating β decays and single neutron additions occurs, indicated by the notched ladders in Fig. 1.7. Nuclides climb these ladders until they reach the next segment of the r-process pathway. Nuclides with neutron magic numbers build to excess abundances, as with the s-process, but they occur at proton-deficient compositions relative to the s-process stability path. Therefore, when the neutron flux falls off and nuclides on the ladders undergo β decay back to the stability line, the r-process local abundance peaks are displaced about 6–12 mass units below

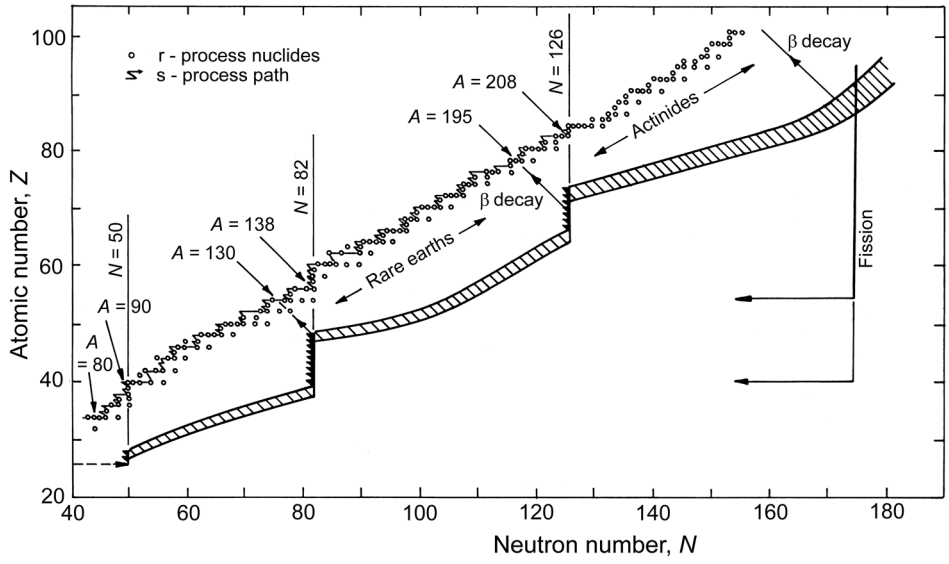

Fig. 1.7 Neutron capture paths of the s-process and r-process shown on the chart of the nuclides. Hatched zone indicates the r-process nucleosynthetic pathway for a plausible neutron flux. Neutron 'magic numbers' are indicated by vertical lines, and mass numbers of nuclide abundance peaks are marked. After Seeger *et al.* (1965).

the s-process peaks (Fig. 1.6). The r-process is terminated by neutron-induced fission at mass 254, and nuclear matter is fed back into the element-building processes at masses of ca. 108 and 146. Thus, cycling of nuclear reactions occurs above mass 108.

Because of the extreme neutron flux postulated for the r-process, its occurrence is probably limited to supernovae. However, Blake and Schramm (1976) proposed the existence of a process that occurred at intermediate neutron fluxes between the s- and r-processes, which they called the 'n-process'. This could occur when neutron addition only slightly exceeds rates of β decay. Although neglected for many years, phenomena similar to the n-process have received consideration in some recent modelling of supernova outflows (Meyer, 2005; Wanajo, 2007; Panov and Janka, 2009).

The effects of r- and s-process synthesis of typical heavy elements may be demonstrated by an examination of the chart of the nuclides in the region of the light rare earths (Fig. 1.8). The step-by-step building of the s-process contrasts with the 'rain of nuclides' produced by β decay of r-process products. Some nuclides, such as ^{143}Nd to ^{146}Nd are produced by both r- and s-processes. Some, such as ^{142}Nd are s-only nuclides 'shielded' from the decay products of the r-process by intervening nuclides. Others, such as ^{148}Nd and ^{150}Nd are r-only nuclides which lie off the s-process production pathway.

Several heavy nuclides from ^{74}Se to ^{196}Hg lie isolated on the proton-rich side of the s-process growth path (e.g. ^{144}Sm in Fig. 1.8), and are also shielded from r-process production. In order to explain the existence of these nuclides it is necessary to postulate a p-process by which normal r- and s-process nuclei are bombarded by protons at very high temperature (>2 × 10^9 K), probably in the outer envelope of a supernova.

1.3 Radioactive Decay

Nuclear stability and decay is best understood in the context of the chart of nuclides. It has already been noted that naturally occurring nuclides define a path in the chart of the nuclides, corresponding to the greatest stability of

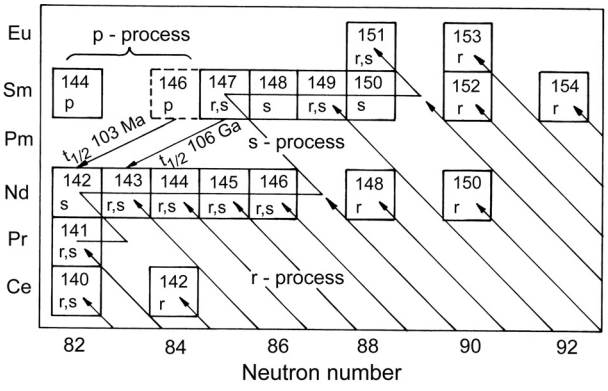

Fig. 1.8 Part of the chart of the nuclides in the area of the light rare earths to show p-, r- and s-process product nuclides. After O'Nions *et al.* (1979).

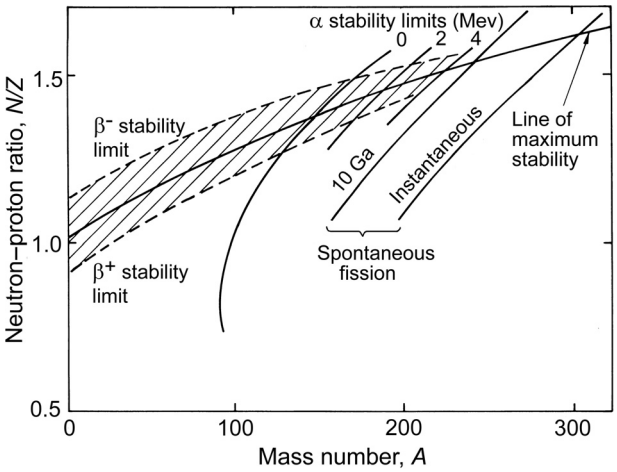

Fig. 1.9 Theoretical stability limits of nuclides illustrated on a plot of N/Z against mass number (A). Lower limits for α emission are shown for α energies of 0, 2 and 4 MeV. Stability limits against spontaneous fission are shown for half-lives of 10 Ga and zero (instantaneous fission). After Hanna (1959).

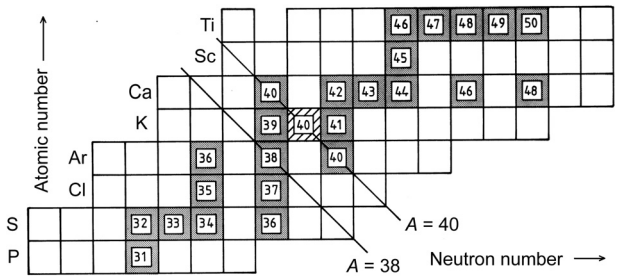

Fig. 1.10 Part of the chart of the nuclides, in coordinates of atomic number (Z) against neutron number (N) in the region of potassium. Stable nuclides are shaded; the long-lived unstable nuclide ^{40}K is hatched. Diagonal lines are isobars (lines of constant mass number, A).

proton/neutron ratio. For nuclides of low atomic mass, the greatest stability is achieved when the numbers of neutrons and protons are approximately equal ($N = Z$), but as atomic mass increases, the stable neutron/proton ratio increases until $N/Z = 1.5$. Theoretical stability limits are illustrated on a plot of N/Z against mass number (A) in Fig. 1.9 (Hanna, 1959).

The path of stability is in fact an energy 'valley' into which the surrounding unstable nuclides tend to fall, emitting particles and energy. This constitutes the process of radioactive decay. The nature of particles emitted depends on the location of the unstable nuclide relative to the energy valley. Unstable nuclides on either side of the valley usually decay by 'isobaric' processes. That is, a nuclear proton is converted to a neutron, or vice versa, but the mass of the nuclide does not change significantly (except for the 'mass defect' consumed as nuclear binding energy). In contrast, unstable nuclides at the high end of the energy valley often decay by emission of a heavy particle (e.g. α particle), thus reducing the overall mass of the nuclide.

1.3.1 Isobaric Decay

Different decay processes indicated on Fig. 1.9 can best be understood by looking at example sections of the chart of nuclides. Figure 1.10 shows a part of the chart around the element potassium. The diagonal lines indicate isobars (nuclides of equal mass) which are displayed on energy sections in Fig. 1.11 and Fig. 1.12.

Nuclides deficient in protons decay by transformation of a neutron into a proton and an electron. The latter is then expelled from the nucleus as a negative 'β' particle (β^-), along with an anti-neutrino ($\bar{\nu}$). The energy released by the transformation is divided between the β particle and the anti-neutrino as kinetic energy (Fermi, 1934). The observed consequence is that the β particles emitted have a continuous energy distribution from nearly zero to the maximum decay energy. Low-energy β particles are very difficult to separate from background noise in a detector, making the β decay constant of nuclides such as ^{87}Rb very difficult to determine accurately by direct counting (Section 3.1).

In many cases the nuclide produced by β decay is left in an excited state which subsequently decays to the ground state nuclide by a release of energy. This may either be lost as a γ ray of discrete energy, or may be transferred from the nucleus to an orbital electron, which is then expelled

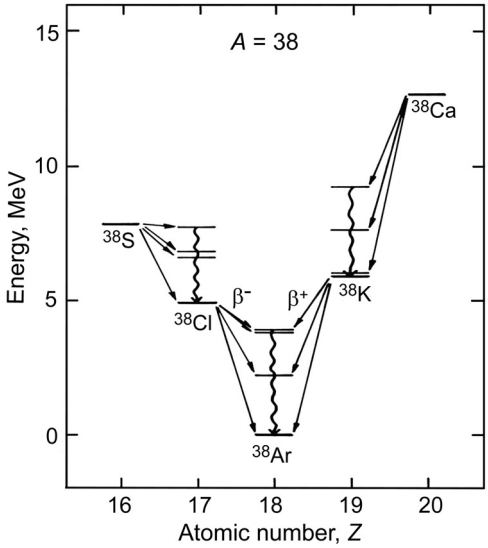

Fig. 1.11 A simple energy section through the chart of nuclides along the isobar $A = 38$ showing nuclides and isomers. Data from Lederer and Shirley (1978).

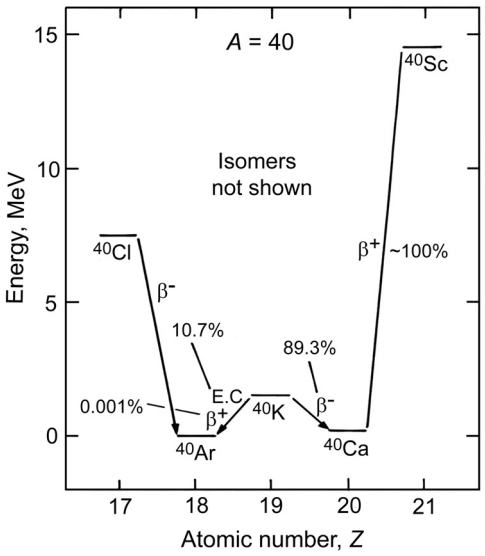

Fig. 1.12 Energy section through the chart of nuclides along isobar $A = 40$. Isomers are omitted for simplicity. For nuclides with more than one decay mechanism the percentage of transitions by different decay routes is indicated. Data from Lederer and Shirley (1978).

from the atom. In the latter case, nuclear energy emission in excess of the binding energy of the electron is transferred to the electron as kinetic energy, which is superimposed as a line spectrum on the continuous spectrum of the β particles. The meta-stable states, or 'isomers' of the product nuclide are denoted by the superscript 'm', and have half-lives from less than a pico-second up to 241 years (in the case of ^{192m}Ir). Many β emitters have complex energy spectra involving a ground state product and more than one short-lived isomer, as shown in Fig. 1.11. The decay of ^{40}Cl can yield 35 different isomers of ^{40}Ar (Lederer and Shirley, 1978), but these are omitted from Fig. 1.12 for the sake of clarity.

Nuclides deficient in neutrons, e.g. ^{38}K (Fig. 1.11), may decay by two different processes: positron emission and electron capture. Both processes yield a product nuclide which is an isobar of the parent, by transformation of a proton to a neutron. In positron emission a positively charged electron (β^+) is emitted from the nucleus along with a neutrino. As with β^- emission, the decay energy is shared between the kinetic energy of the two particles. After having been slowed down by collision with atoms, the positron interacts with an orbital electron, whereby both are annihilated, yielding two 0.511 MeV γ rays (this forms part of the decay energy of the nuclear transformation).

In electron capture decay (EC) a nuclear proton is transformed into a neutron by capture of an orbital electron, usually from one of the inner shells, but possibly from an outer shell. A neutrino is emitted from the nucleus, and an outer orbital electron falls into the vacancy produced by electron capture, emitting a characteristic X-ray. The product nucleus may be left in an excited state, in which case it decays to the ground state by γ emission.

When the transition energy of a decay route is less than the energy equivalent of the positron mass ($2m_eC^2 = 1.022$ MeV), decay is entirely by electron capture. Thereafter, the ratio β^+/EC increases rapidly with increasing transition energy (Fig. 1.12), but a small amount of electron capture always accompanies positron emission even at high transition energies.

It is empirically observed (Mattauch, 1934) that adjacent isobars cannot be stable. Since ^{40}Ar and ^{40}Ca are both stable species (Fig. 1.10), ^{40}K must be unstable, and exhibits a branched decay to the isobars on either side (Fig. 1.12).

1.3.2 Alpha and Heavy Particle Decay

Heavy atoms above bismuth in the chart of nuclides often decay by emission of an α particle, consisting of two protons and two neutrons (He^{2+}). The daughter product is not an isobar of the parent, and has an atomic mass reduced by four. The product nuclide may be in the ground state, or remain in an excited state and subsequently decay by γ emission. The decay energy is shared between kinetic energy of the α particle and recoil energy of the product nuclide.

The U and Th decay series are shown in Fig. 12.1. Because the energy valley of stable proton/neutron ratios in this part of the chart of the nuclides has a slope of less than unity, α decays tend to drive the products off to the neutron-rich side of the energy valley, where they undergo β decay. In fact β decay may occur before the corresponding α decay.

At intermediate masses in the chart of the nuclides, α decay may occasionally be an alternative to positron or electron capture decay for proton-rich species such as ^{147}Sm. However, α decays do not occur at low atomic numbers because the path of nuclear stability has a Z/N slope close to unity in this region (Fig. 1.1). Any such decays would simply drive unstable species along (parallel to) the energy valley.

An exotic mode of radioactive decay was discovered in the ^{235}U to ^{207}Pb decay series (Rose and Jones, 1984), whereby ^{223}Ra decays by emission of ^{14}C directly to ^{209}Pb with a decay energy of 13.8 MeV. However this mode of decay occurs with a frequency of less than 10^{-9} of the α decay of ^{223}Ra.

1.3.3 Nuclear Fission and the Oklo Natural Reactor

The nuclide ^{238}U (atomic no. 92) undergoes spontaneous fission into two product nuclei of different atomic number, typically ca. 40 and 55 (Zr and Cs), along with various other particles and a large amount of energy. Because the heavy parent nuclide has a high neutron/proton ratio, the daughter products have an excess of neutrons and undergo isobaric decay by β emission. Although the frequency of spontaneous fission of ^{238}U is less than 2×10^{-6} that of α decay, in heavier transuranium elements spontaneous fission is the

principal mode of decay. Other nuclides, such as ^{235}U, may undergo fission if they are struck by a neutron. Furthermore, since fission releases neutrons which promote further fission reactions, a chain reaction may be established. If the concentration of fissile nuclides is high enough, this leads to a thermonuclear explosion, as in a supernova or atomic bomb.

In special cases where an intermediate heavy-element concentration is maintained, a self-sustaining but non-explosive chain reaction may be possible. This depends largely on the presence of a 'moderator'. Energetic 'fast' neutrons produced by fission undergo multiple elastic collisions with atoms of the moderator. They are decelerated into 'thermal' neutrons, having velocities characteristic of the thermal vibration of the medium, the optimum velocity for promoting fission reactions in the surrounding heavy atoms. One natural case of such an occurrence is known, termed the Oklo natural reactor (Cowan, 1976; Naudet, 1976).

In May 1972, ^{235}U depletions were found in uranium ore entering a French processing plant and traced to an ore deposit at Oklo in the Gabon Republic of central Africa. In spite of its apparent improbability, there is overwhelming geological evidence that the ^{235}U depletions were caused by the operation of a natural fission reactor at around 1.8 Ga. It appears that in the Early Proterozoic, conditions were such that the series of coincidences needed to create a natural fission reactor were achieved more easily than at the present day.

Uranium dispersed in granitic basement was probably eroded and concentrated in stream-bed placer deposits. It was immobilized in this environment as the insoluble reduced form due to the nature of prevailing atmospheric conditions. With the appearance of blue-green algae, the first organisms capable of photosynthesis, the oxygen content of the atmosphere, and hence river water, probably rose, converting some reduced uranium into more soluble oxidized forms. These were carried down-stream in solution. When the soluble uranium reached a river delta it must have encountered sediments rich in organic ooze, creating an oxygen deficiency which again reduced and immobilized uranium, but now at a much higher concentration (up to 0.5% uranium by weight).

After burial and compaction of the deposit, it was subsequently uplifted, folded and fractured, allowing oxygenated ground waters to re-mobilize and concentrate the ores into veins over 1 m wide of almost pure uranium oxide. Hence the special oxygen fugacity conditions obtaining in the Proterozoic helped to produce a particularly concentrated deposit. However, its operation as a reactor depended on the greater ^{235}U abundance (3%) at that time, compared with the present day level of 0.72%, reduced by α decay in the intervening time (half-life = 700 Ma).

In the case of Oklo, light water (H_2O), must have acted as a moderator, and the nuclear reaction was controlled by a balance between hot water loss by convective heating or boiling, and replacement by cold groundwater influx. In this way the estimated total energy output (15 000 mega-watt years, representing the consumption of six tons of ^{235}U) was probably maintained at an average of only 20 kW for about 0.8 Ma.

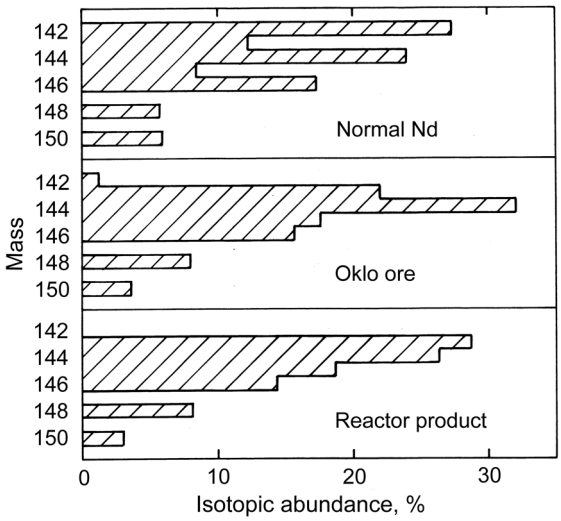

Fig. 1.13 Bar charts of the isotope composition in normal Nd, Oklo ore and reactor fission product waste. Data from Cowan (1976).

Geochemical evidence for the occurrence of fission is derived firstly from the characteristic elemental abundances of fission products. For example, excess concentrations of rare earths and other immobile elements such as Zr are observed. Alkali metal and alkaline earths were probably also enriched, but have subsequently been removed by leaching. Secondly, the characteristic isotope abundances of some elements can only be explained by fission (Raffenach *et al.*, 1976).

The Nd isotope composition of the Oklo ore is very distinctive (Fig. 1.13). ^{142}Nd is shielded from isobaric decay of the neutron-rich fission products (Fig. 1.8) so that its abundance indicates the level of normal Nd. After correction for an enhanced abundance of ^{144}Nd and ^{146}Nd due to neutron capture by the large-cross-section nuclides ^{143}Nd and ^{145}Nd, Oklo Nd has an isotopic composition closely resembling that of normal reactor fission product waste (Fig. 1.13).

Evidence for a significant neutron flux is also demonstrated by the isotope signatures of actinide elements. For example, the abundant isotope of uranium (^{238}U) readily captures fast neutrons to yield an appreciable amount of ^{239}U, which decays by β emission to ^{239}Np and then ^{239}Pu (Fig. 1.14). The latter decays by α emission with a half-life of 24 ka to yield more ^{235}U, contributing an extra 50% to the 'burnable' fuel, as in a 'fast' breeder reactor ('fast' refers to the speed of the neutrons involved). Because the fission products of ^{239}Pu and ^{235}U have distinct isotopic signatures, it is determined that very little ^{239}Pu underwent neutron-induced